DETECTION OF EXTRA-SOLAR PLANETS WITH GROUND-BASED TELESCOPES

Steven H. Pravdo[1]

Jet Propulsion Laboratory

Mail Stop 306-438

California Institute of Technology

Pasadena, CA 91109

and

Stuart B. Shaklan[1]

Jet Propulsion Laboratory

Mail Stop 306-388

California Institute of Technology

Pasadena, CA 91109

submitted to the *Astrophysical Journal* October 20, 1994

---

[1]The research described in this paper was carried out in part by the Jet Propulsion Laboratory, California Institute of Technology, under contract with the National Aeronautics and Space Administration.

ABSTRACT

The detection of extra-solar planets around stars like the Sun remains an unfulfilled goal of astronomy. We describe a program called Single-Telescope Extra-Solar Planet Survey, or *STEPS*, that can perform a statistically significant search for Jupiter-mass planets around nearby stars using a large-aperture ground-based telescope. We consider sources of measurement noise including photon noise, atmospheric motion between stars, sky background, instrumental noise, and differential chromatic refraction, to simulate results. In 10 night yr^{-1} of observations we can search 88 nearby stars for Jupiter-mass planets with a 10-m telescope. We show how an increase in the length of the observing program expands the parameter spaces that are searched--orbital periods and semi-major axes. The properties of the stars used in the simulation come from the Gliese & Jahreiss catalog of nearby stars. Since the survey is time- and not source-limited the number of stars surveyed increases with the observing time. We describe an instrument, a CCD camera, suitable for this program. The ultimate limit for this system that could be used for a small number of target stars is ~100 μas astrometric precision.

Subject headings: stars: planetary systems

1. INTRODUCTION

The question "Do other stars have planets?" is of interest to scientists and non-scientists alike. The answer in scientific terms is not easy, however, because even if extra-solar planets are ubiquitous no one has yet successfully detected one. Continuing observations of nearby stars using various techniques including astrometry (e.g. Gatewood 1987) and radial velocity measurements (e.g. Latham et al. 1989, Cochran et al. 1991, Marcy et al. 1993, McMillan et al. 1994) have to date yielded only upper limits to the masses of possible planets. Some false alarms of planet detections have turned out to be discoveries of low-mass binary companion stars. Other inferred planet detections (Marsh and Mahoney 1992, 1993) are subject to alternative interpretations (Boss & Yorke 1993). The detection of planets around a pulsar (Wolszczan & Frail 1992) is on firmer ground (but see Gil et al. 1993, Peale 1993), but may be unrelated to the solar-like planetary systems that we consider herein. In summary, as of now, there are no known planets orbiting main sequence stars other than the Sun.

Both theoretical models and observational evidence lead us to conclude that the solar system is not the result of an improbable path of stellar evolution and therefore, that planetary systems are common. Black & Matthews (1985) and Levy et al. (1990) compile much of the theoretical work on solar system formation and the observational evidence. The observations describe an evolutionary chain from protostars, through pre-main sequence stars, to stars like the Sun. Circumstellar disks (e.g. Smith & Terrile 1984) are a common phenomenon in young stars which may be the precursors of planetary systems.

The planets are believed to have formed in the protosolar nebula (e.g. Safronov 1969). The solar system is organized into two types of planets: gas giants (Jupiter, Saturn, Uranus, Neptune) and terrestrial planets (Earth, Mars, Venus, Mercury). Gas giants form beyond the water-

condensation radius, a distance from the center of the nebula beyond which water and other abundant volatiles remain solid (e.g. Safronov & Ruskol 1994), while terrestrial planets form within this radius. Pluto is an anomaly. Gas giants are also 10-300 times more massive than terrestrial planets because more planet-forming material is available at their locations. Based on the solar model, the astrometric search for gas giants is easier than for terrestrial planets because they are more massive and further from the star, both contributors to larger astrometric signals.

The search for planetary systems has contributed to the development of instruments and techniques designed to solve the difficult problem of planet detection. Burke et al. (1993) is a compendium of these proposals. In this paper we describe a new experiment to survey nearby stars for planets using a large-diameter ground-based telescope. We call the experiment *STEPS*, for Single-Telescope Extra-solar Planet Survey.

2. PLANET DETECTION TECHNIQUE

We will search for planets around nearby stars by astrometrically measuring the motion of the stars around their planetary system center-of-mass. Consider the simplest case of a single planet orbiting a single star. Then the astrometric signal Θ (Figure 1) of the star is:

$$\Theta\ (\mu\text{as}) = 960 * (a / 5\ \text{a.u.}) * (d / 10\ \text{pc}) * (M_P / M_J) * (M_\odot / M_S) \qquad (1)$$

where a is the semi-major axis of the planetary orbit, d is the distance to the star, (M_P/M_J) is the planet-to-Jupiter mass ratio, and $(M_S / M_\odot)$ is the stellar mass in solar units. The period T of the planet is:

$$T\,(\mathrm{yr}) = 11 * (a / 5\ \mathrm{a.u.})^{1.5} * (M_S / M_\odot)^{0.5} \qquad (2)$$

A current astrometric program (Gatewood et al. 1990) achieves accuracies on the order of 1000 μas and is thus capable of detecting Jupiter-like planets around some stars. Note that the orbital period is an important observational parameter since it defines the observing program length and, for fixed M_S, Θ is proportional to $T^{0.67}$.

We measure the position of a target star relative to a surrounding field of reference stars. These stars form a fixed frame of reference from which changes in position of the target star are determined. This technique was described by Eichhorn & Williams (1963) and is employed by Gatewood (1987). The reference stars allow us to make an affine transformation between observations (e.g. Shaklan et al. 1994a). At least three reference stars are required to generate a linear model of the field; six reference stars for a quadratic model. Since we also solve for the parallaxes and proper motions of the reference stars, an additional reference star is required for either model. With the small fields discussed below (Section 5) a linear model is usually sufficient. In any case with more reference stars, the field model is more robust. The field model accounts for optical aberrations to a level below that of the required accuracy.

The astrometric data Σ from the target star corrected to the solar barycenter and which we simplify from two dimensions to one can be written:

$$\Sigma(t) = (\Theta / 2) * \sin(2\pi t / T + \phi) + \mu * t + P * \sin(2\pi t) + c + \sigma_0 \qquad (3)$$

where t is the time of observation, ϕ is the orbital phase at time zero, μ is the proper motion, P is the parallax, and c is the mean position. σ_0 is the standard deviation of the noise per observation. It is estimated from the data by determining the exposure-to-exposure target star motion relative to the reference stars. One can detect a planetary signal in a time sequence of such data in a number of ways including Fourier or periodigram (Black & Scargle 1982) analysis. We have chosen to analyze the data by performing a least squares fit of the five parameters in equation 3. This analysis allows us to determine the probability that the detected signal is not simply a noise artifact. To do this, we first create a simulated 10-yr data set containing non-zero values for all five parameters and a noise of σ_0 per measurement. We use typical values of μ and P of 1 asec yr^{-1} and 0.1 asec, respectively. Uncertainties in P are reduced to an acceptable level with 1 observation yr^{-1} if the observations are distributed within a $\pm$ 20 day window. This yields an estimated amplitude, period, and phase for the stellar motion. We then perform a non-existence test on the measured amplitude by setting Θ to zero, fixing the period and phase to that obtained in the simulation, and generating new 10-yr data sets. For each data set, we obtain an estimated amplitude having a Gaussian distribution with standard deviation σ_Θ. The probability that the amplitude determined from the first simulation is due strictly to noise is given by the erf function (e.g. Press et al. 1989) evaluated at Θ/σ_Θ. Figure 2 shows the $3\sigma_\Theta$ values plotted vs. T for data that consists of one observation/yr for 10 yr with σ_0 of 400 μas. For T $\leq$ 10 yr the values are independent of ϕ. For T > 10 yr the $3\sigma_\Theta$ values correspond to observations with the worst possible ϕ; i.e. with the most linear portion of the sinusoid centered at T/2. Figure 2 can be interpreted in the following way: any stellar astrometric signal above the curve is a planet detection with at least 3σ confidence. The figure clearly shows the penalty for measuring

periods that exceed the duration of the observing program. A search for Jupiter-mass planets around solar-type stars should have a duration of at least 11 years to avoid this penalty.

3. TARGET STARS

As shown in (1) the astrometric signal depends inversely on the distance to the star. Thus nearby stars are the best candidates to search for planets using this method. Our source catalog for stars within ~25 pc of the Sun is the *Preliminary Version of the Third Catalogue of Nearby Stars* or CNS3 (Gliese & Jahreiss 1993). CNS3 contains 3802 stars including 3 B, 73 A, 264 F, 486 G, 772 K, and 1097 M stars. We also treat 639 stars with color class "m" as M stars based upon their colors and absolute luminosities. Stellar distances are determined from the given trigonometric parallaxes or in some cases photometric and spectroscopic parallaxes. Stellar masses are determined using the relation:

$$\log (M_s / M_\odot) = 0.118 * (4.75 - M_{bol}) \qquad (4)$$

with the stellar bolometric magnitude, M_{bol} , taken from the spectral type, luminosity class, and bolometric corrections (Allen 1973). For stars where the luminosity class or subtype is not given, we assume luminosity class V and subtype 0.5. Stars with color types of "m" are assumed to be M5 dwarfs for the mass estimates. This is consistent with their absolute luminosities.

We begin with the 3229 *CNS3* stars which have $\Theta \geq 300$ μas with a Jupiter-mass planet and $T \leq 10$ yr. Any of these stars could in principle be detected at 3σ with the ultimate *STEPS* precision but as described below (Section 8) much more time than the survey allows would be required. We

further restrict this sample for two reasons. First, to limit the effects of differential chromatic refraction (DCR; see Section 6) we use a ±16° swath in declination around the site of the ground-based observatory. We chose 20 ±16° for the Keck observatory. Second, to insure enough reference stars in each field (Section 5), we limit the galactic latitude of the target stars to $b^{II} \leq 30°$. This results in 430 candidates, consisting of 3 A, 22 F, 55 G, 85 K, 148 M, and 117 m stars. Figure 3 shows the astrometric signals for these stars assuming Jupiter-mass planets in 10-year orbits, plotted in descending signal magnitude.

We have not undertaken to separate these candidates into single stars and multiple star systems (binaries and others). The few that are known short-period binaries (T < 10 yr) will be removed. Other short period binaries will be discovered by this survey and eliminated when appropriate. Long-period binaries both known and discovered are not expected to be different from single stars in the properties of their planetary systems. In studies of a subset of *CNS3* less than 3% of the stars were in long period binary systems (Wasserman & Weinberg 1991).

4. *STEPS* INSTRUMENT

The proposed instrument is a CCD camera. We discuss two possible implementations: one which requires a custom CCD chip mosaic and another that can make use of a single large-format chip. In both cases the imaging area is a 6.144 cm square. The custom chip mosaic is shown in Figure 4 and summarized in Table 1. It contains five CCDs that are built on the same substrate. The substrate is thinned to illuminate the chip from the backside and increase the quantum efficiency. The four outer CCDs are identical in design but oriented as shown. They contain 1048 x 1000 pixels that are 30 μm squares. The central CCD is considerably smaller, 48 x 48 pixels, also 30 μm squares.

The large pixels are appropriate for the image sizes from large ground-based telescopes (see Section 5) and also provide large full wells for dynamic range. The purpose of the central CCD is to further increase the camera dynamic range by viewing with it bright target stars with shorter exposures and faster readouts. Since the chips are on the same substrate relative astrometry between chips is as good as astrometry within one large-format chip.

The single large-format chip is 4096 x 4096 with 15 μm square pixels, an existing format. Table 2 summarizes the properties of this CCD. The chip is operated in a partially inverted mode to maximize the full well. To match the image sizes pixels are summed on-chip into 2 x 2 subarrays. The standard chip is front-side illuminated with significantly less quantum efficiency than the custom mosaic. A chip with properties listed in Table 2 is well within the state-of-the-art (e.g. Janesick et al. 1989).

The imager is sealed with a transparent window that is smooth to $\lambda/20$. This makes the astrometric motions due to thickness gradients in the window negligible. The camera electronics are standard (e.g. Stubbs et al. 1993) with the addition of software selectable sub-windows (~10 regions of 50 x 50 30-μm pixels, or 100 x 100 15-μm pixels) that can be read out while dumping the charge from the rest of the pixels. This will allow us to operate at 50 kpixel s^{-1} within the noise requirements. The camera has a shutter and filter wheel. The filter wheel has three positions, two for DCR filters (Section 6), and one for the astrometric filter with which astrometric data are taken. The astrometric filter is also smooth to $\lambda/20$.

Astrometric data will be read in the windows containing the target and reference stars. We estimate 10 windows × 2500 pixels × 12 bits × 600 frames = 180 Mbits of data per night.

5. TELESCOPES AND SITES

We compared the performance of three telescopes and sites to determine the effect of telescope diameter and other parameters on the *STEPS* experiment. We considered the 1.5- and 5-m telescopes of Palomar Observatory and the 10-m telescope of Keck Observatory. Table 3 lists the relevant parameters for the comparison.

For the three telescopes considered the fields-of-view are determined by balancing two competing effects. First the atmospheric noise in the relative astrometric signal between stars is proportional to their separation in the small angle limit (see Section 6). This leads toward smaller fields. Contrariwise, the number of reference stars is proportional to the area in a field. The more reference stars, the better the field model can be determined (e.g. Eichhorn & Williams). A minimum of four reference stars is required to determine a linear model of the field and solve for the reference star parallaxes and proper motions. For small fields and small optical aberrations a linear model is usually sufficient. In some cases a quadratic model gives better results. This requires at least seven reference stars. At the Keck telescope, the proposed 2048 x 2048 x 30 μm pixel format has a field of view of 84 asec, yielding an average of 8.6 reference stars with $V \leq 21$ at $b^{II} = 30°$ (Allen 1973). A limiting magnitude of $V = 21$ was chosen because these are the faintest stars that can be used as statistically significant reference stars in the observations. Smaller fields using fainter stars suffer from photometric noise. Larger fields having brighter reference stars have more atmospheric noise. This is borne out in Figure 5.

In the analysis discussed below and for Figure 5, the centroid noise is computed by fitting a Gaussian profile to the image with a weighted-least-squares algorithm. The weight of each pixel in

the sum of the squared residuals is given by the summed variances of shot noise, read noise, and sky background. The algorithm is discussed in some detail by Stone (1989).

For purposes of comparison between the 10-, 5-, and 1.5-m telescopes, we choose fields-of-view that have the same average number of reference stars. While Figure 5 shows that there is a slight penalty to be paid for $V = 21$ compared to $V = 20$, we have chosen the former for our limiting magnitude because the smaller field is more tolerant of optical aberrations and it fits on a standard large-format CCD chip.

Astrometric accuracy can be limited by optical aberrations, especially distortion (Gatewood 1992). Figure 6 shows the as-designed distortion for the Keck 10 m across the *STEPS* field of view. The telescope has low intrinsic distortion and also low sensitivity to motion of the secondary mirror (Figure 6). These effects are negligible compared to other sources of error discussed below (Sections 6-8). The 1.5- and 5-m telescopes are similarly well-behaved.

Another issue for the Keck 10-m is the effect of the primary segments on astrometry. Note that aberrations on the primary do not change astrometric performance since all stars are affected in the same way. The Keck segments are actively aligned to 50 masec. For 36 segments this implies that any centroid motion due to one segment will be 1400 μas. Therefore to achieve astrometric accuracy at the ~100 μas level we require that *differential* effects due to segment misalignments be no more than ~10% of the overall centroid motion. This is expected to be the case since segment misalignments are well within the seeing disk diameter.

6. ATMOSPHERIC EFFECTS

Atmospheric effects are important limits for high-precision ground-based astrometry. Lindegren (1980) shows that the astrometric motion between two stars separated by angle θ due to the atmosphere is proportional to θ^{-1} in the narrow angle regime; $\theta \ll 0.2°$ in most cases. In addition, the motion varies with aperture diameter, $D^{-2/3}$ (Shao & Colavita 1992). Observational evidence confirms this behavior (Gatewood 1991, Colavita 1994, Dekany et al. 1994). For the Keck 10 m and separations of 42 asec (*STEPS* field-of-view radius) the atmospheric motion between stars is 220 μas √hr.

Differential chromatic refraction (DCR) is another important effect of the atmosphere which results in relative astrometric errors (e.g. Monet et al. 1992). This occurs because bluer stars refract more than red stars at non-zero zenith angles. We calibrate DCR for our reference fields in the following way. We observe broadband in the visible avoiding water absorption bands in the near infrared. We then estimate the blackbody temperatures of the target and reference stars in the field by observing them with two off-the-shelf bandpass filters in the λ530-570 nm and λ680-720 nm bands. Note that these filters fall within the astrometric filter band. Figure 7 shows a blackbody spectrum fit to the filter results of an observation of a G4 V star. Analysis shows that the intrinsic error is about 100 μas for stars in the O5 to M5 range. Using the DCR filter data with 1% photometry the residual effect of DCR is reduced to 180 μas per observation at 16° zenith angle. To achieve this residual or better we limit observations to zenith angles between ± 16°.

7. CCD DATA ANALYSIS

Astrometric data analysis on CCDs has been discussed by Monet & Dahn (1983). We determine relative centroid positions of stellar images on the chip to perform relative astrometry. To achieve an astrometric accuracy of, for example, 100 μas requires a centroid accuracy of 0.0024 pixel. This requirement is eased by the fact that the stellar images are spread over many pixels. Seeing-limited images on the Keck 10-m will spread over ~ 570 pixels, the image full width ($[2 \times 0.5$ asec/0.042 asec/pixel$]^2$). Thus the centroid accuracy on each pixel is $0.0024 \times \sqrt{570} = 0.057$, well within current capabilities (Monet et al. 1992).

Systematic errors in pixel locations due to, for example, step and repeat errors in the CCD fabrication, will also introduce errors into the astrometric analysis. Shaklan & Pravdo (1994) discuss a method to calibrate such systematic errors. Shaklan & Pravdo (1994) and Shaklan et al. (1994b) have demonstrated calibration accuracies in excess of the *STEPS* requirements. Buffington et al. (1990) has shown that CCD photometric and dimensional stabilities are more than adequate for the *STEPS* experiment.

8. *STEPS* PROGRAM AND RESULTS

Given target and reference stars, a proposed instrument (the CCD mosaic), telescope performances, and a model for atmospheric effects, we are ready to describe an observing program and present the results of our end-to-end model. In the *STEPS* program we will observe candidate stars for extra-solar planets a minimum of 10 nights yr^{-1}. Since the survey is time- and not source-limited the number surveyed increases with available observing time. Again, as a practical issue (availability of telescope dark time) we assume a bright sky for these simulations. The observing

efficiency due to bad weather and other effects, is conservatively chosen to be 50%, resulting in a net observing time of 30 hr yr^{-1}. The program will last for 10-20 yr, a necessity considering the range of orbital periods in the search. Target stars will be observed once or twice per year. At a minimum, observations are made annually distributed within ± 20 day intervals to permit parallax solutions. This sampling imposes a lower limit to the period search of $T \gtrsim 2$ yr. The DCR calibration observations will be performed infrequently and do not add much overhead to the program. They could even be done at an alternate site.

As noted in Section 2, the ability to detect a planet around a star with a given data set depends upon the astrometric signal Θ, the period T, and in some cases the phase ϕ. In what follows all stars are observed with equal time regardless of their expected Θ. Also for T greater than the program length we assume the worst possible (i.e. making the astrometric motion hardest to detect) value for ϕ. Figure 8 shows how our accuracy per observation of 405 μas is attained. The observation time/source is iterated until a total time of 30 hr is used and 3σ results are obtained for the observed sources in a parameter range of interest (see Figure 9 and following).

In these simulations we assume that the noise on the target star centroid estimation is limited by the noise on the faintest useful reference star in the field ($V = 21$ at Keck, $V = 19$ at the 5-m, $V = 18$ at the 1.5-m). This is a conservative assumption because, on average, 5.4 of the 8.6 reference stars are at least a full magnitude brighter than the faintest one. On the other hand, it allows for the integration time penalty associated with the order (linear or quadratic) of the field model (Shaklan & Pravdo 1993), as well as flexibility in discarding peculiar reference stars.

Figure 9 shows the detectable periods (3σ) for stars observed with the 1.5-, 5-, and 10-m telescopes in a 10-yr program. This demonstrates the utility of a larger aperture: in equal programs

the 10-m observes 88 stars compared to 29 for the 5-m, 9 for the 1.5-m. At the end of the 10-20 year program (see below) it is important to have searched a statistically significant sample of stars.

The stars in Figure 9 are plotted in order of decreasing astrometric signal, Θ. If a star has a larger Θ because it is closer and less massive, then with an equal-time observation, more "orbital-period space" is searched. Since the only known "Jupiter"-star period is 11.9 yr, it is important to search as much of this space as possible. Note that for half of the stars, period ranges of at least 5-10 years are searched with the 10-m. Figure 10 is a companion plot that shows the orbital semi-major axes that are searched. The utility of the backside-illuminated advanced CCD mosaic with higher quantum efficiency is illustrated in Figure 11. It increases both the number of target stars and the bright star parameter space; the latter since fewer readouts of the reference star frames reduce the noise.

The 10-m telescope will observe a significant sample of 88 stars. If there are no detections in this program we can conclude that Jupiter-mass planets are uncommon in this sample. Let us examine the properties of this sample more closely. These consist of 44 M (3 M0, 3 M1, 8 M2, 13 M3, 12 M4, 3 M5, 2 M6) and 44 m stars with average derived masses of 0.27 and 0.19 $M_\odot$, respectively. Figure 12 shows a histogram of these masses. Theoretical modeling has yet to answer the question whether such stars, 2.5-10 times less massive than the Sun, can have Jupiter-mass planets. Jupiter contains approximately 0.001 of the present solar system mass. Jupiter-mass planets around the survey stars would contain 0.0025-0.01 of the system mass.

Figure 13 shows the effect of program length on the searched parameter space for the 10-m telescope. If, as suggested, the water-condensation radius beyond which gas giants form is at about

5 a.u. independent of stellar temperature (Boss 1994), then this figure shows the value of a 20 year program since 5 a.u. is searched for 85 of the 88 program stars.

If the survey is allowed more time per year, the number of sources observed increases but not linearly with time. This is shown in Table 4. The reason for diminishing returns is that the signals of the added sources are smaller than that of the originally observed targets. Other targets with higher signals could be included by relaxing the declination and galactic latitude constraints. For example, 122 sources could be observed in 10 night yr^{-1} between declinations -12 to 52° .

Higher mass stars could be observed in a more limited program. Figure 14 shows that 25 stars with $0.4\ M_\odot < M < 0.6\ M_\odot$ could be observed over a limited area of parameter space in the 10-m, , 10-yr, 10 night yr^{-1} program. Stars more massive than $0.6\ M_\odot$ pose an interesting observational problem. In the ordering of astrometric signals for the declination- and galactic latitude-limited sample (Figure 3) the first star with $M > 0.6\ M_\odot$ is Procyon. It is ranked 58th with a signal of 1749 μas for a 10-yr period and would fall within the nominal *STEPS* program (except for its $V = 0.4$; see below) which cuts off at ~1350 μas. The next star is Altair, ranked 125th with a signal of 1127 μas. There are only 36 stars with $M > 0.6\ M_\odot$ anywhere in the sky with signals as large as 1200 μas. An added complication with these stars is their magnitude range: $-1.4 < V < 7.1$. Scattering in the optics leads to high background for the reference stars and would be a significant problem for these bright targets. The dynamic range of at least 3×10^5 (with the $V = 21$ reference stars) would also be challenging. Astrometry using photometers (Gatewood 1987) or radial velocity searches (e.g. McMillan et al. 1994) may be better suited to these stars.

Figure 15 shows the error budget for the ultimate astrometric precision of this system, 101 μas, obtained with 10 hr observations per source. Clearly a small number of sources could be observed in this way.

9. CONCLUSION

We have described a program that allows us to make a statistically significant survey of nearby stars for Jupiter-mass planets. The experiment uses an existing ground-based telescope and a CCD mosaic, but could use with some degradation a standard-type CCD camera. The number of stars, ~ 88, in the 10 night yr^{-1} survey, is important because we expect to detect several Jupiter-mass planets in so large a sample if the canonical model of solar system formation is correct. Note that the probabilities for false positives are 0.19, 0.02, 2×10^{-3}, and 1×10^{-4} for 1, 2, 3, and 4 detections, respectively. Systems with detected Jupiter-mass planets are prime targets for terrestrial planet searches.

If no Jupiter-mass planets are found we can conclude with 99.99% confidence that gas-giant planets as large (or larger) than Jupiter form in at most 10% of the systems . Since we do not search the same areas of parameter space for each star this conclusion is an approximation. The absence of detectable Jupiter-mass planets would begin to put pressure on the theory that planetary systems like the solar system are common, at least for stars in the surveyed mass range.

We acknowledge Mark Colavita, George Gatewood, Anthony Gleckler, Hiroshi Kadogawa, Eugene Levy, David Monet, and Michael Shao for useful discussions.

Table 1. Advanced *STEPS* CCD Mosaic Properties

Outer Chips Format	1048 x 1000
Central Chip Format	48 x 48
Pixel Size	30 μm x 30 μm
Quantum Efficiency	60% at λ700 nm
System Throughput	0.35
Full Well	750,000 e^-
Mode	Partially Inverted
Read Noise	5 e^-
Dark Current	« 2 e^- pix^{-1} s^{-1}
Operating Temp.	-70° C

Table 2. *STEPS* CCD Properties

Format	4096 x 4096
Pixel Size	15 μm x 15 μm
Quantum Efficiency	43% at λ700nm
System Throughput	0.25
Full Well	185,000 e^-
Mode	Partially Inverted
Read Noise	5 e^- pix^{-1}
Dark Current	« 2 e^- $pix^{-1}s^{-1}$
Operating Temp.	-70° C

Table 3. Telescope Comparisons for *STEPS*

Primary Diameter	**1.5 m**	**5 m**	**10 m**
Image Scale (asec/30μm-pix)	0.476	0.078	0.042
Field-of-View Diameter (asec)	178	133	84
Reference Star *V* Mag	18	19	21
Number Ref. Stars ($b^{II} = 30°$)	8.6	8.6	8.6
Sky (bright sky mag $asec^{-2}$)	19	19	20
Seeing FWHM (asec)	1.0	1.0	0.5

Table 4. Number of Target Stars vs. Observing Nights per Year

Nights yr^{-1}	**Target Stars**
5	65
10	88
20	122
30	144
40	159

REFERENCES

Allen, C. W. 1973, Astrophysical Quantities, (Ethylene Press: London)

Black, D. C. & Matthews, M. S. 1985, Protostars and Planets II, (U. of Arizona Press: Tucson, Space Science Series)

Black, D. C. & Scargle, J. D. 1982, Ap. J., 263, 854

Boss, A. P. 1994, submitted for publication

Boss, A. P. & Yorke, H. W. 1993, Ap. J., 411, L99

Buffington, A. et al. 1990, P. A. S. P., 102, 688

Burke, B. F. et al. 1993, TOPS: Toward Other Planetary Systems, Solar System Exploration Division Report, NASA publication.

Cochran, W. D. et al. 1991, Ap. J. (Letters), 380, L35

Colavita, M. M. 1994, A. Ap., 283, 1027

Dekany, R. et al. 1994, Ap. Sp. Sci., 212, 299

Eichhorn, H. K. & Williams, C. A. 1963, A. J., 68, 221

Gatewood, G. 1987, A. J., 94, 213

Gatewood, G. 1991, B. A. A. S., 23, 1433

Gatewood, G. 1992, in Astrometric Imaging Telescope 1991 Final Report (ed. S. Pravdo, JPL publication D-9651), 85

Gil, J. A. et al. 1993, A. Ap., 271, L17

Gliese, W. & Jahreiss, H. 1993, Preliminary Version of the Third Catalogue of Nearby Stars (CNS3), preprint

Jacoby, G. H. et al. 1984, Ap. J. Suppl., 56, 257

Janesick, J. et al. 1989, in CCDs in Astronomy, A. S. P. Conference Series No. 6

Latham, D. W. et al. 1989, Nature, 339, 38

Levy, E. H. et al., 1992, Protostars and Planets III, (U. of Arizona Press: Tucson, Space Science Series)

Lindegren, L. 1980, A. Ap., 89, 41

Marcy, G. W. et al. 1993, Remote Sensing Rev., 8, 205

Marsh, K. A. & Mahoney, M. J. 1992, Ap. J., 395, L115

_____. 1993, Ap. J., 405, L71

McMillan, R. S. et al. 1994, Ap. Sp. Sci., 212, 271

Monet, D. et al. 1992, A. J., 103, 638

Monet, D. & Dahn, C. C. 1983, A. J., 88, 1489

Peale, S. J. 1993, A. J., 105, 1562

Press, W. H. et al. 1989, Numerical Recipes, (Cambridge: Cambridge University Press)

Safronov, V. S. 1969, Evolution of the Protoplanetary Cloud and Formation of the Earth and the Planets (Moscow: Nauka)

Safronov, V. S. & Ruskol, E. L., Ap. Sp. Sci., 212, 13

Shaklan, S. et al. 1994a, Ap. Sp. Sci., 212, 453

Shaklan, S. & Pravdo, S. H. 1993, S. P. I. E, 1945, 505

Shaklan, S. & Pravdo, S. H. 1994, S. P. I. E., 2198, 1227

Shaklan, S. et al. 1994b, submitted to Appl. Opt.

Shao, M. & Colavita, M. M. 1992, A. Ap., 262, 353

Smith, B. A. & Terrile, R. J. 1984, Sci., 226, 1421

Stone, R. C. 1989, A. J., 97, 1227

Stubbs, C. W. et al. 1993, Proc. S. P. I. E., 1900, 121

Wasserman, I. & Weinberg, M. D. 1991, Ap. J., 382, 149

Wolszczan, A. & Frail, D. A. 1992, Nature, 355, 145

Figure 1. Planet-star configuration illustrating the astrometric signal produced.

Figure 2. Minimum peak-to-peak amplitude of stellar motion for 3σ detection vs. the orbital period of the planet. This plot assumes 1 observation/yr for 10 yrs. Each observation has a precision of 400 μas. For periods longer than 10 years, the curve shows the worst-case phase.

Figure 3. Astrometric signals of all targets stars in the 4 to 36° Declination range with $b^{II} \leq 30°$ assuming a Jupiter-mass planet in a 10-yr orbit. Barnard's Star with a signal of 14500 μas is left out to limit the scale.

Figure 4. Configuration of Advanced *STEPS* CCD mosaic with five CCDs on the same substrate.

Figure 5. Noise in the centroid estimate at a 10-m telescope. The field-of-view (FOV) diameter is chosen so that the total number of reference stars is 8.6 where V is the magnitude of the dimmest reference star. Thus, the left side of the figure represents large fields while the right side is small fields. The FOV diameter for $V = 21$ is 84 asec. The solid curve shows the total effect of shot noise, read noise, and sky background for the faintest reference star used. The dashed curve is the r.m.s. atmospheric turbulence between the center of the field (where the reference star is assumed to be) and 0.7 of the FOV diameter. This curve represents the average amount of atmospheric noise in the field. Larger fields with bright reference stars have more atmospheric noise and less photometric noise. The optimum occurs near $V = 20$. This figure assumes a seeing full-width-half-maximum of 0.5 arcsec.

Figure 6. Distortion at the Keck telescope. The solid curve is the as-designed distortion across an 84 asec field-of-view. The other curves show how the distortion changes when the secondary mirror is misaligned. All three curves are well below the accuracy required for the *STEPS* program.

Figure 7. Differential Chromatic Refraction calibration. The jagged curve is the spectrum of a G4V star (Jacoby et al. 1984) as it would appear when observed through the astrometric bandpass filter on a frontside-illuminated CCD. The solid curve shows a blackbody fit to spectral measurements at 500 ± 20 and 700 ± 20 nm. The fit closely matches the spectrum. The difference between the fit and the spectrum results in a 100 μas astrometric error at a zenith distance of 16°.

Figure 8. Astrometric error budget at the Keck telescope. Atmospheric turbulence contributes 155 μas $\sqrt{}$ hour at 0.7 of the 84 asec field-of-view. Observation of a $V = 21$ reference star adds another 145 μas. This assumes a CCD with quantum efficiency of 0.35. The *STEPS* program surveys 88 sources. Assuming 50% observing efficiency and 10 nights/yr, each source is allocated 20.5 minutes of observation/yr. Combining the noise/observation with the random error associated with DCR results in a noise/observation of 405 μas.

Figure 9. Parameter space available for 3σ detection in a 10-yr program at the 10-, 5-, and 1.5-m telescopes. Equal time is allocated to each source. The shaded area represents the orbital period space that could be explored with 3σ confidence.

Figure 10. Same as Fig. 9 but for semi-major axis. After 10 years of the program, the Keck telescope has explored the 1-3 a.u. region of about 40 stars. Stars appear in the same order as in Fig. 9. The jaggedness of the plot compared to Fig. 9 is due to varying distances and masses of the stars. (Semi-major axis is an absolute parameter; angular motion shown in Fig. 9 is a relative parameter that is directly observed.)

Figure 11. Comparison of the backside-illuminated (i.e. higher quantum efficiency) advanced CCD mosaic with the standard CCD. The stars for which the standard CCD observes constricted areas of parameter space are the bright stars. These require more readouts and thus higher noise to avoid saturation because of the large dynamic range between the target and reference stars.

Figure 12. Histogram of stellar masses in the 10-yr, 10 day/yr, 10-m survey using the CCD mosaic.

Figure 13. Increasing parameter space as a function of program length. The darkest shaded region is identical to the 10-m region in Figure 10. A 15-yr program begins to explore the region beyond 5 a.u. for about 1/4 of the program stars. A 20-yr program reaches 5 a.u. for 85 stars.

Figure 14. Parameter space explored in a survey of high-mass stars in a 10-yr program with a 10-m telescope. This survey is limited to stars with $M > 0.4\ M_\odot$. The small signal associated with these stars makes them difficult to observe, limiting both the sample size and parameter space.

Figure 15. Ultimate astrometric precision of the Keck telescope. A program with 10 hr of observation/source/yr achieves a centroid accuracy of 67 μas. DCR calibration is improved from 180 μas to 75 μas by using spectrophotometric measurements rather than fitting to blackbody curves.

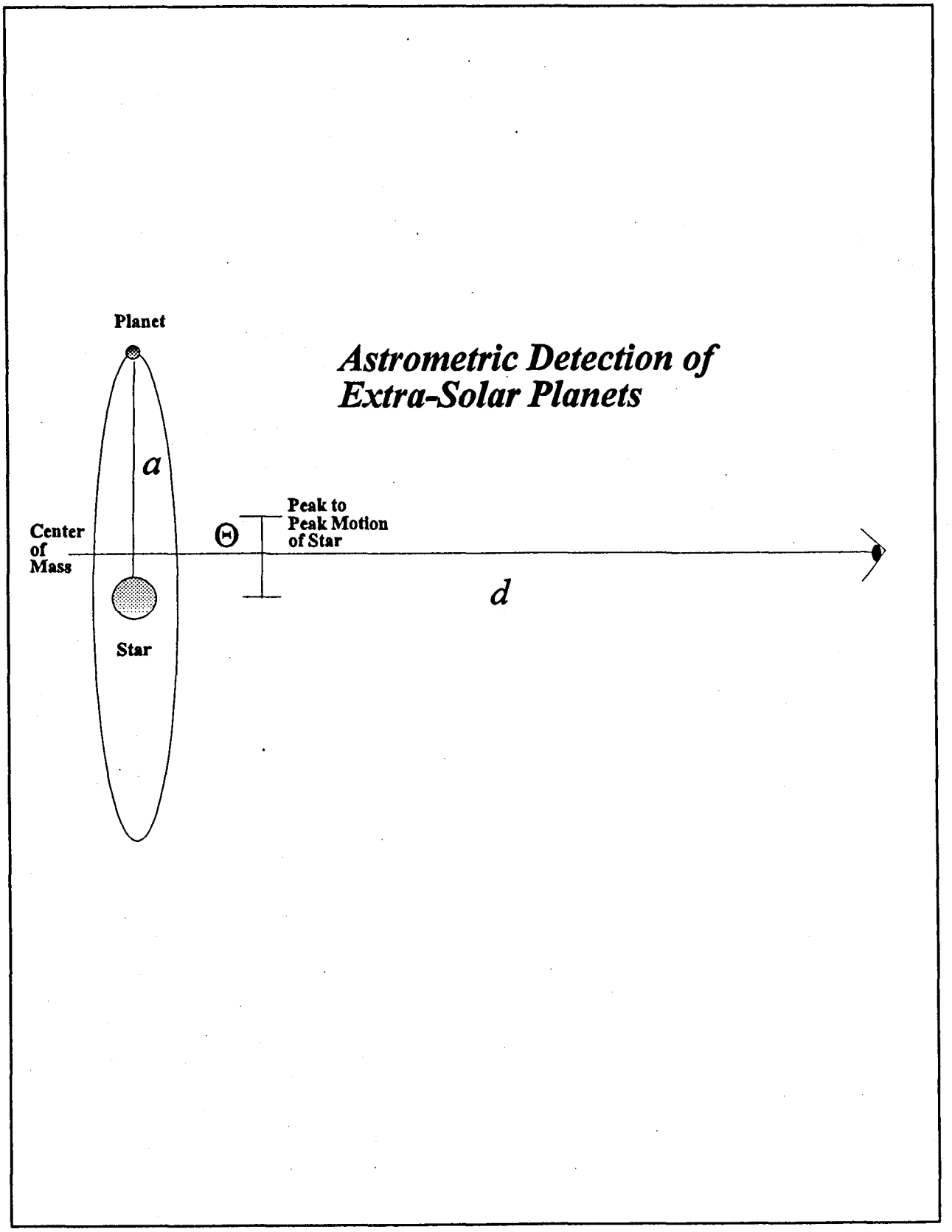

Figure 1. Planet-star configuration illustrating the astrometric signal produced.

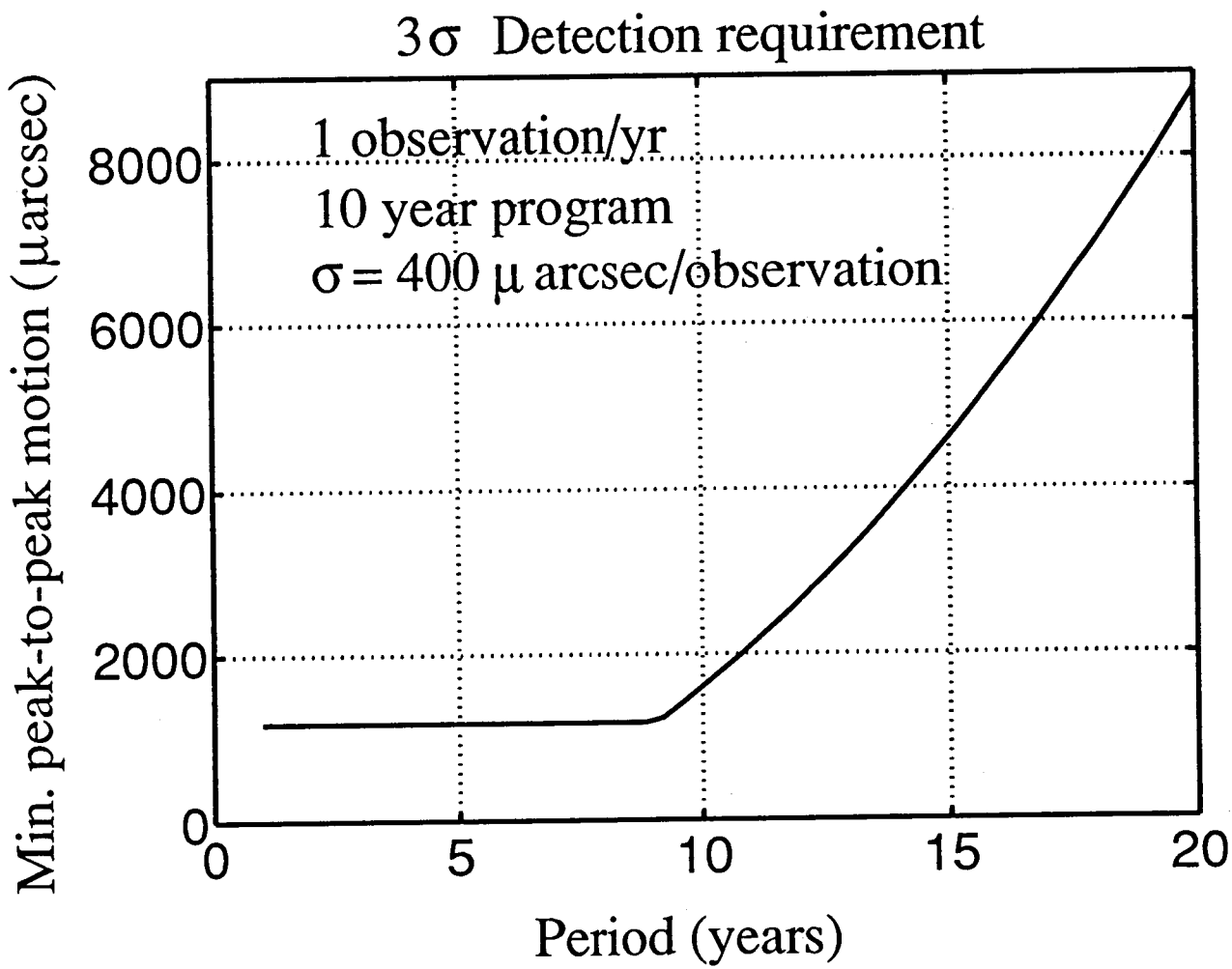
3σ Detection requirement
1 observation/yr
10 year program
σ = 400 μ arcsec/observation
Min. peak-to-peak motion (μarcsec)
8000
6000
4000
2000
0
0
5
10
15
20
Period (years)

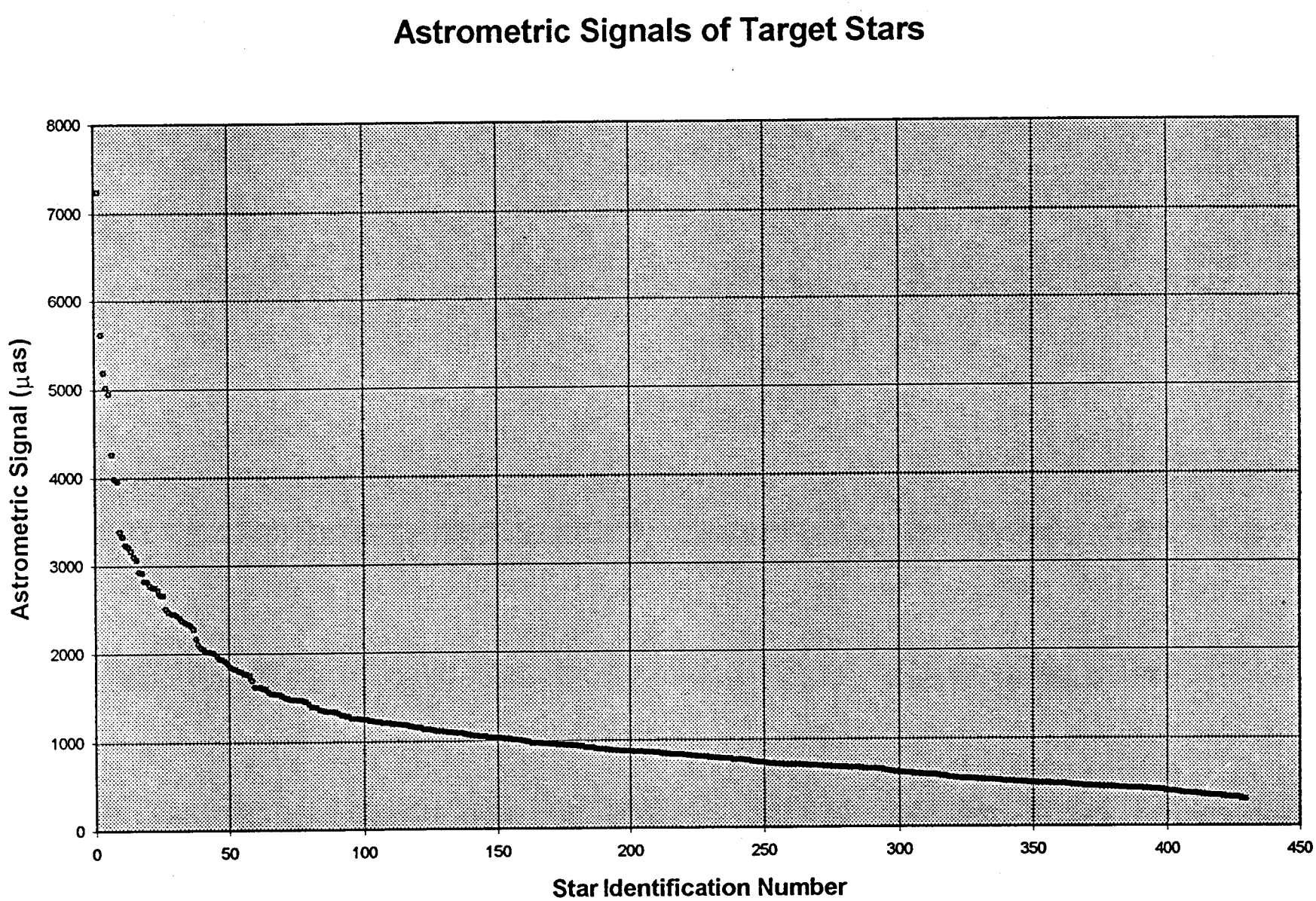

Figure 3. Astrometric signals of all targets in the 4 to 36° dec range with b″ <30° assuming a Jupiter-mass planet in a 10-yr orbit. Barnard's Star (14500 μas) is left out.

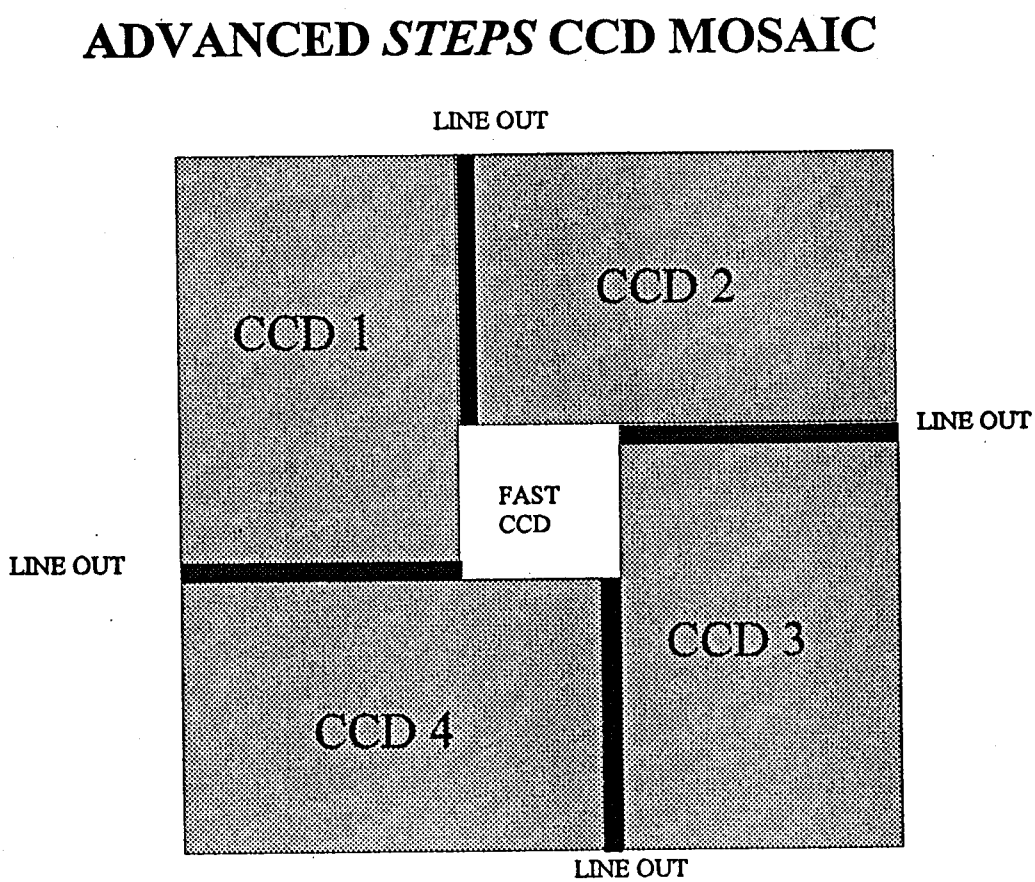

Figure 4. Configuration of Advanced *STEPS* CCD with five CCDS on the same substrate.

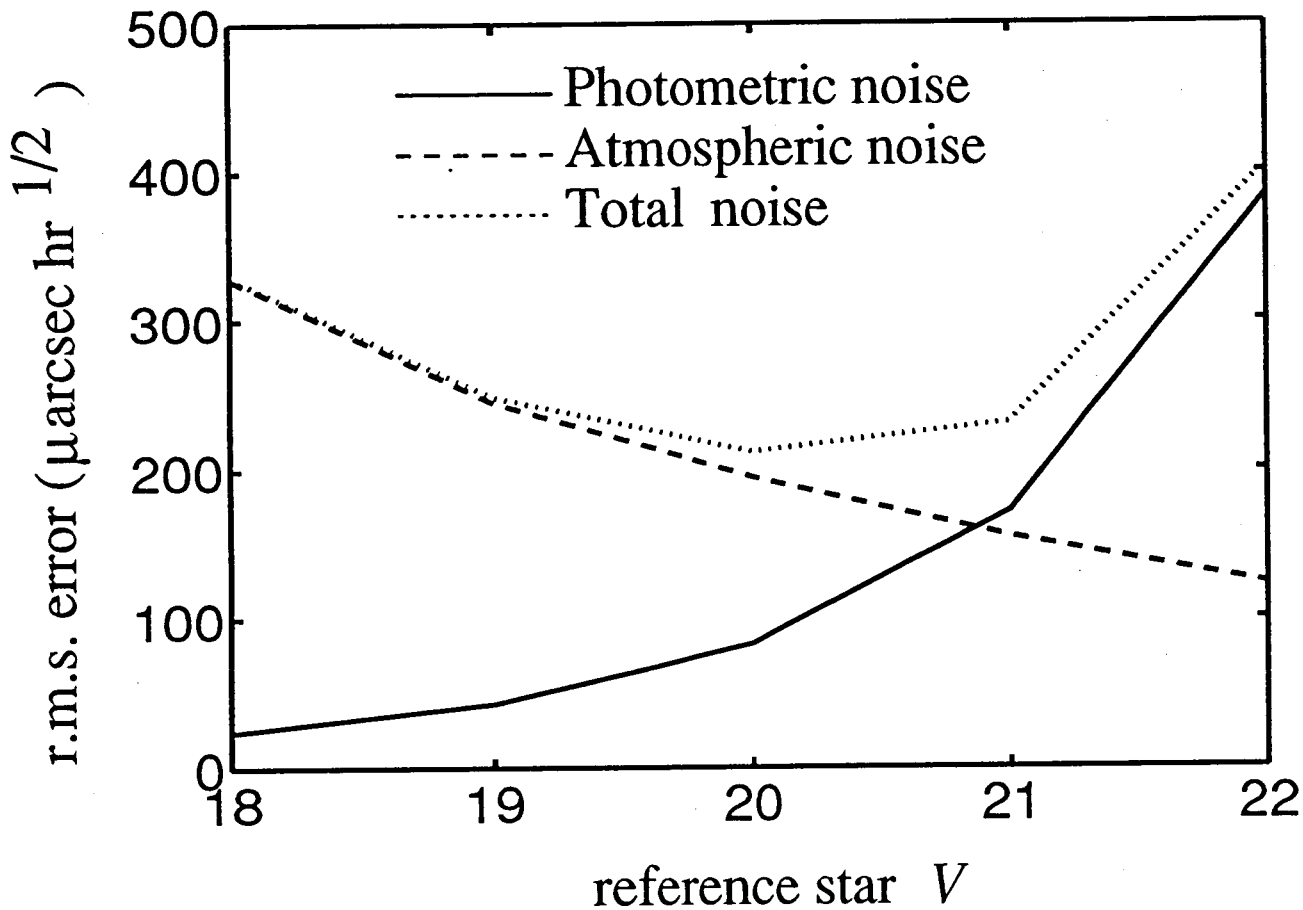
Photometric noise
Atmospheric noise
Total noise
r.m.s. error (μarcsec hr 1/2)
500
400
300
200
100
0
18
19
20
21
22
reference star V

Fig 5

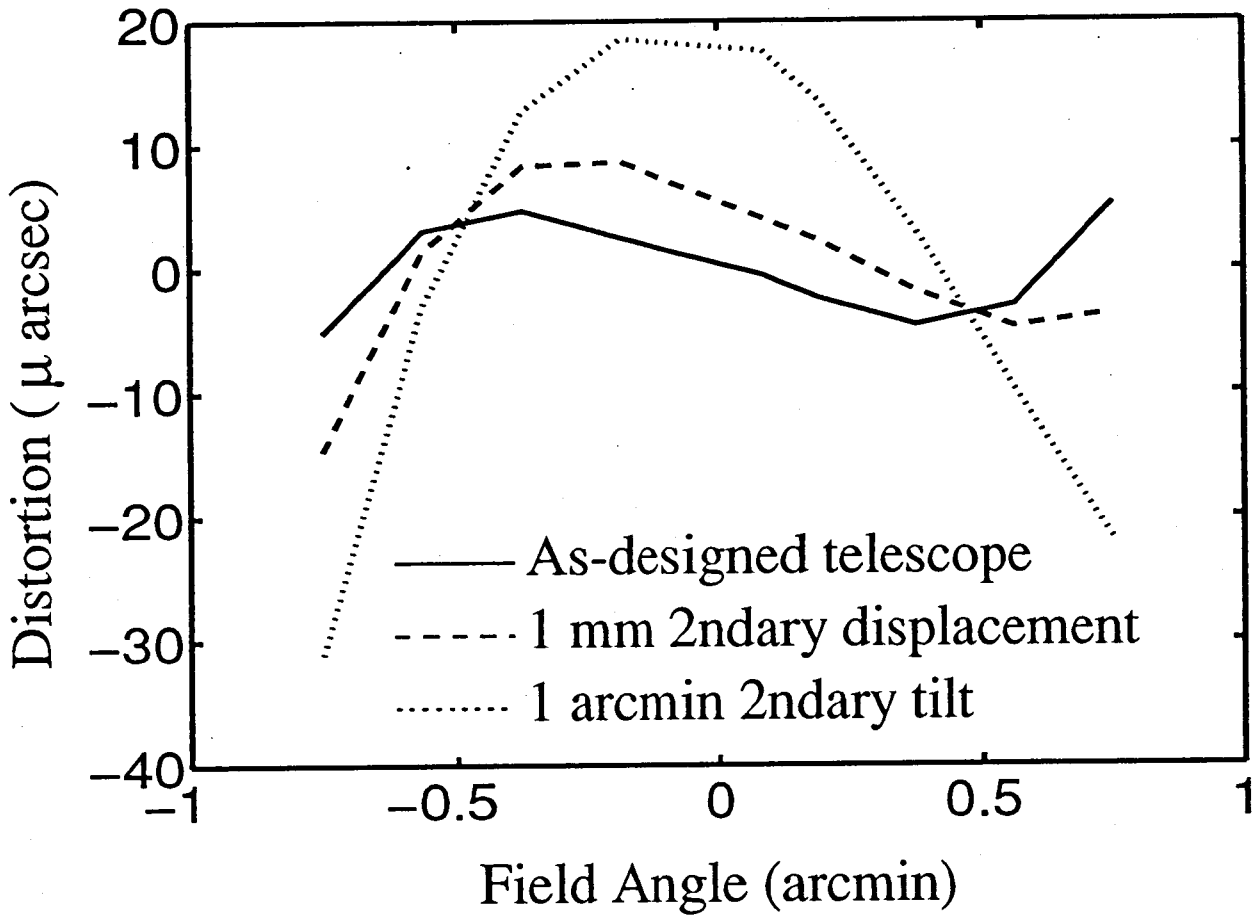
20
10
0
−10
−20
−30
−40
−1
−0.5
0
0.5
1
Distortion (μ arcsec)
Field Angle (arcmin)
As-designed telescope
1 mm 2ndary displacement
1 arcmin 2ndary tilt

Fig 6

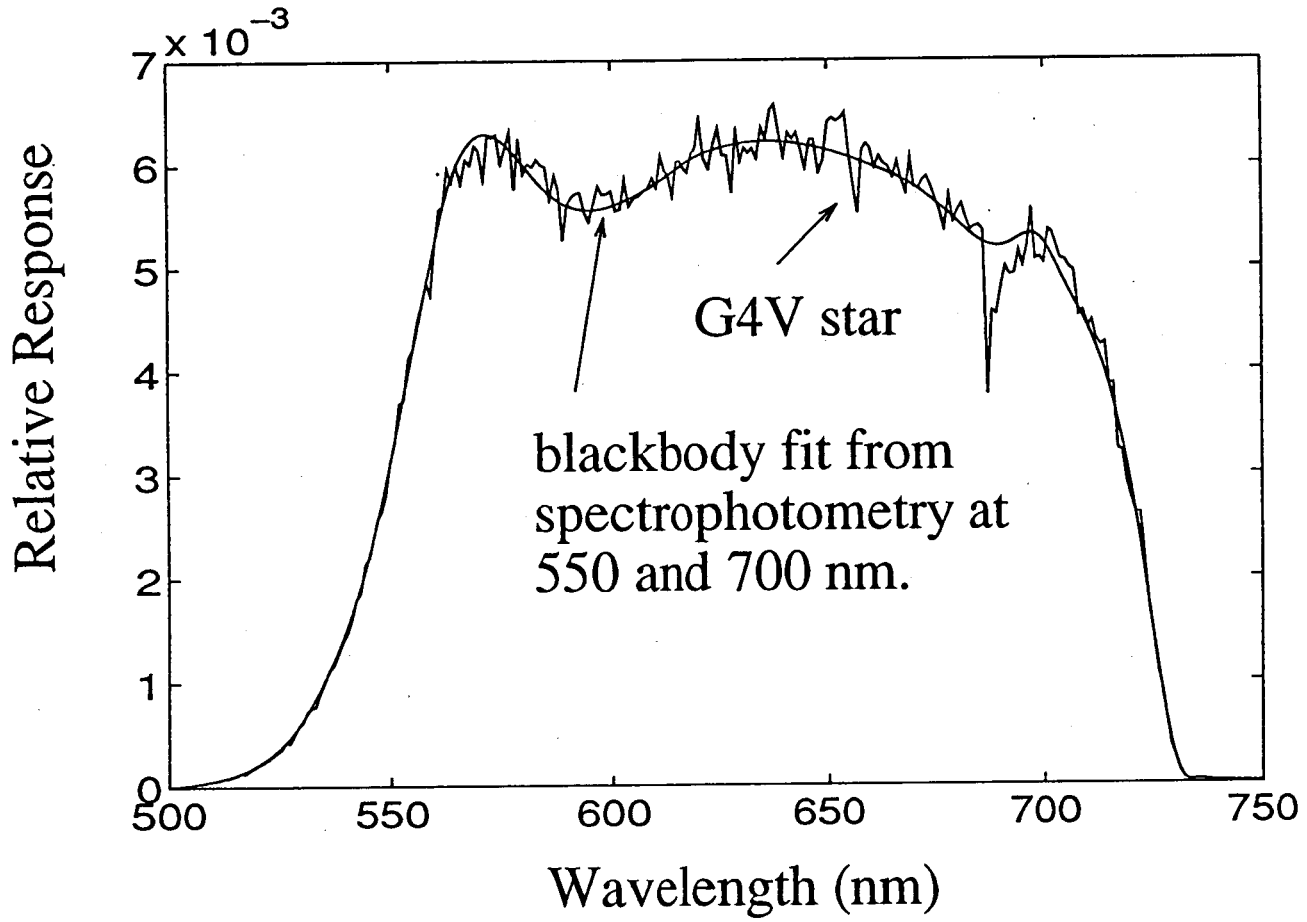
x 10^-3
7
6
5
4
3
2
1
0
500
550
600
650
700
750
Relative Response
Wavelength (nm)
G4V star
blackbody fit from
spectrophotometry at
550 and 700 nm.

Fig 7

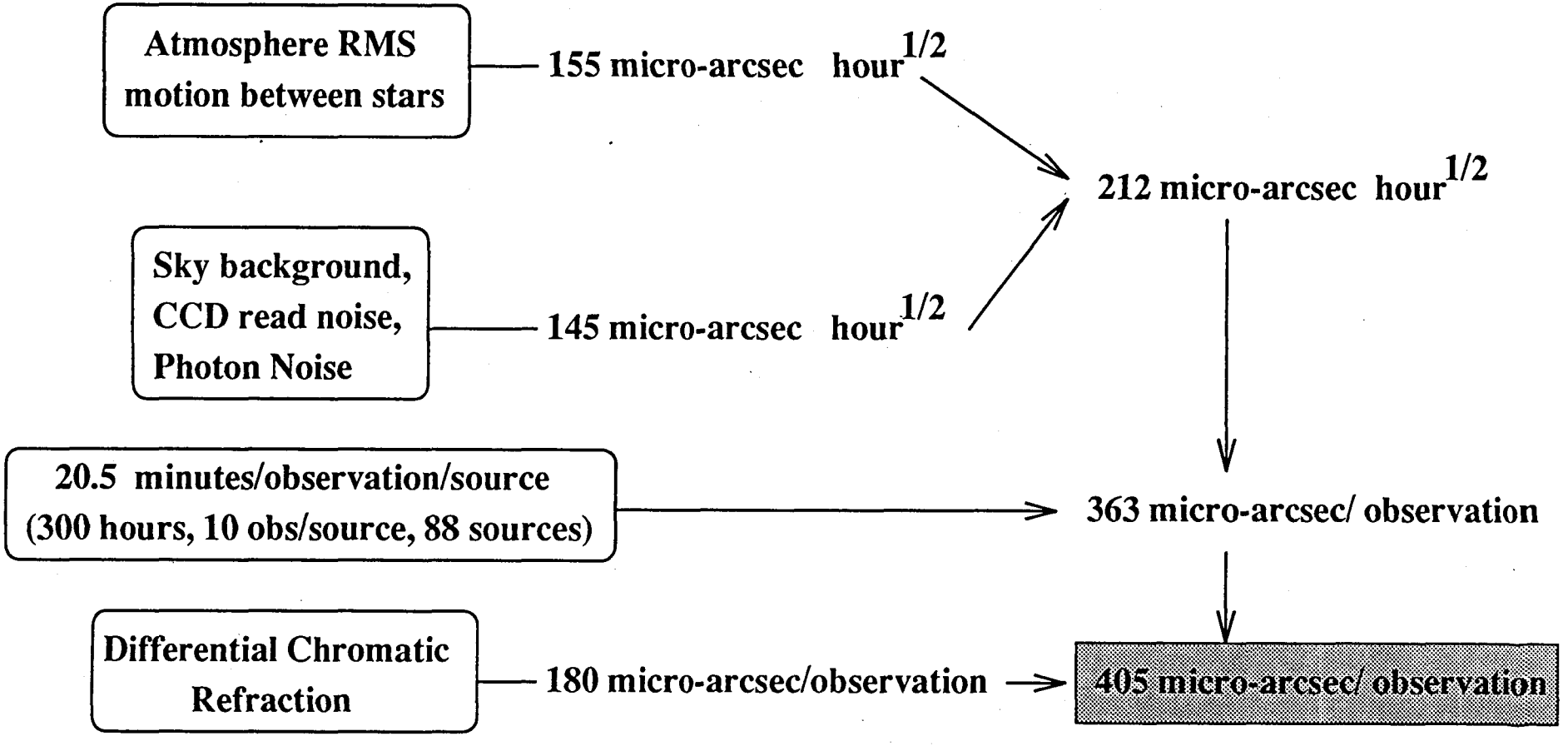
Atmosphere RMS motion between stars
155 micro-arcsec hour^1/2
Sky background, CCD read noise, Photon Noise
145 micro-arcsec hour^1/2
212 micro-arcsec hour^1/2
20.5 minutes/observation/source (300 hours, 10 obs/source, 88 sources)
363 micro-arcsec/ observation
Differential Chromatic Refraction
180 micro-arcsec/observation
405 micro-arcsec/ observation

Fig 8

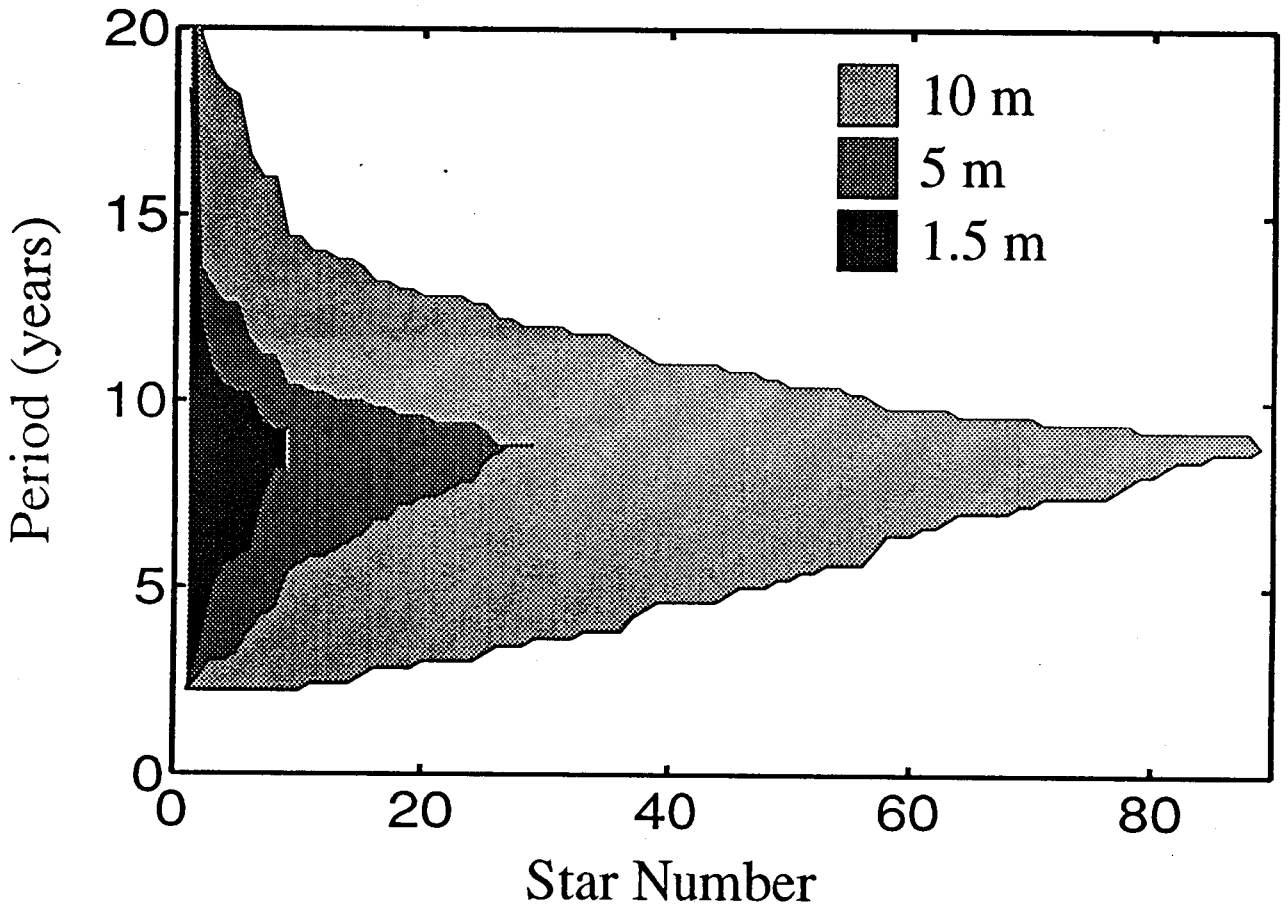

Fig 9

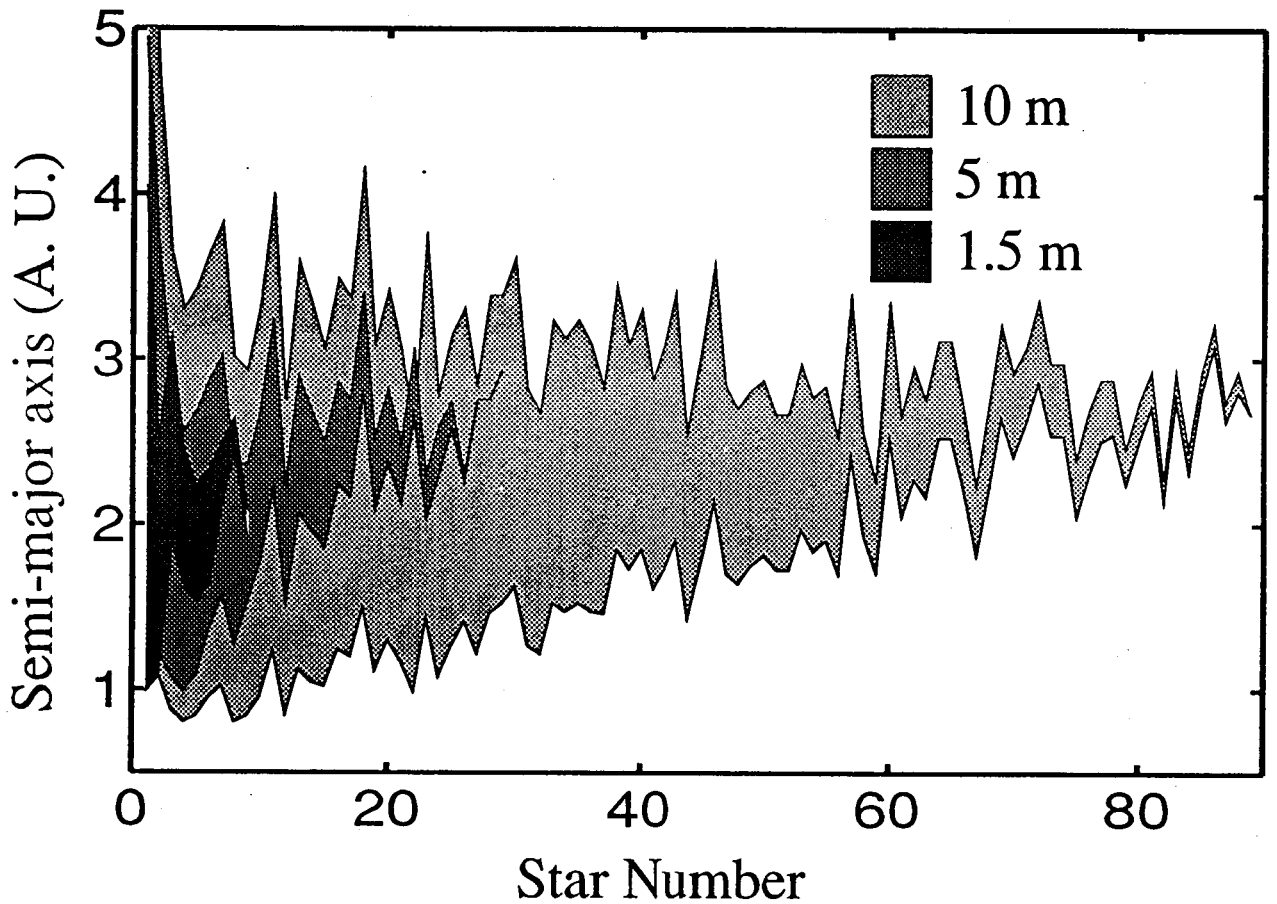
10 m
5 m
1.5 m
Semi-major axis (A. U.)
Star Number
0
20
40
60
80
1
2
3
4
5

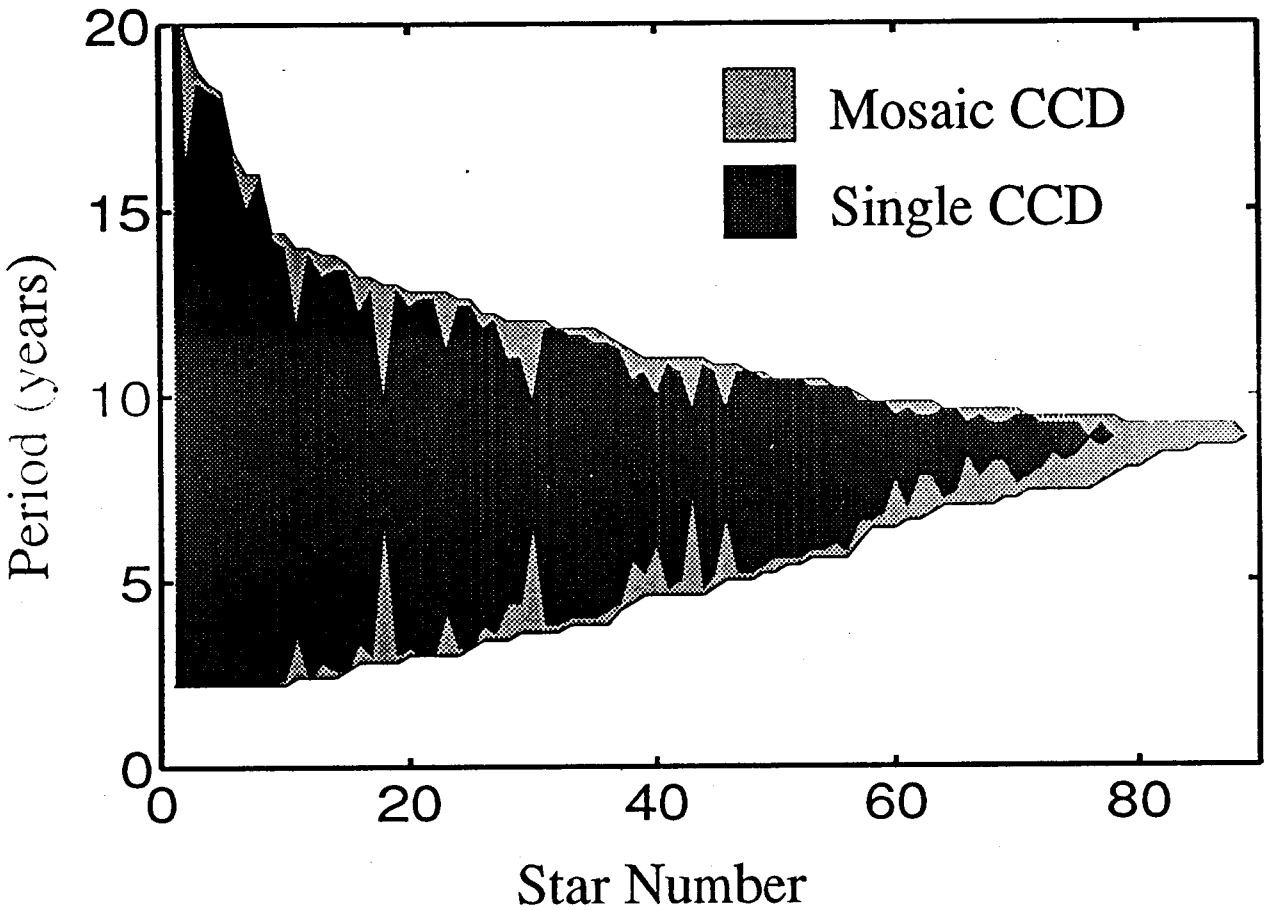
Mosaic CCD
Single CCD
Period (years)
Star Number
0
5
10
15
20
0
20
40
60
80

Histogram of Stellar Masses in the Survey

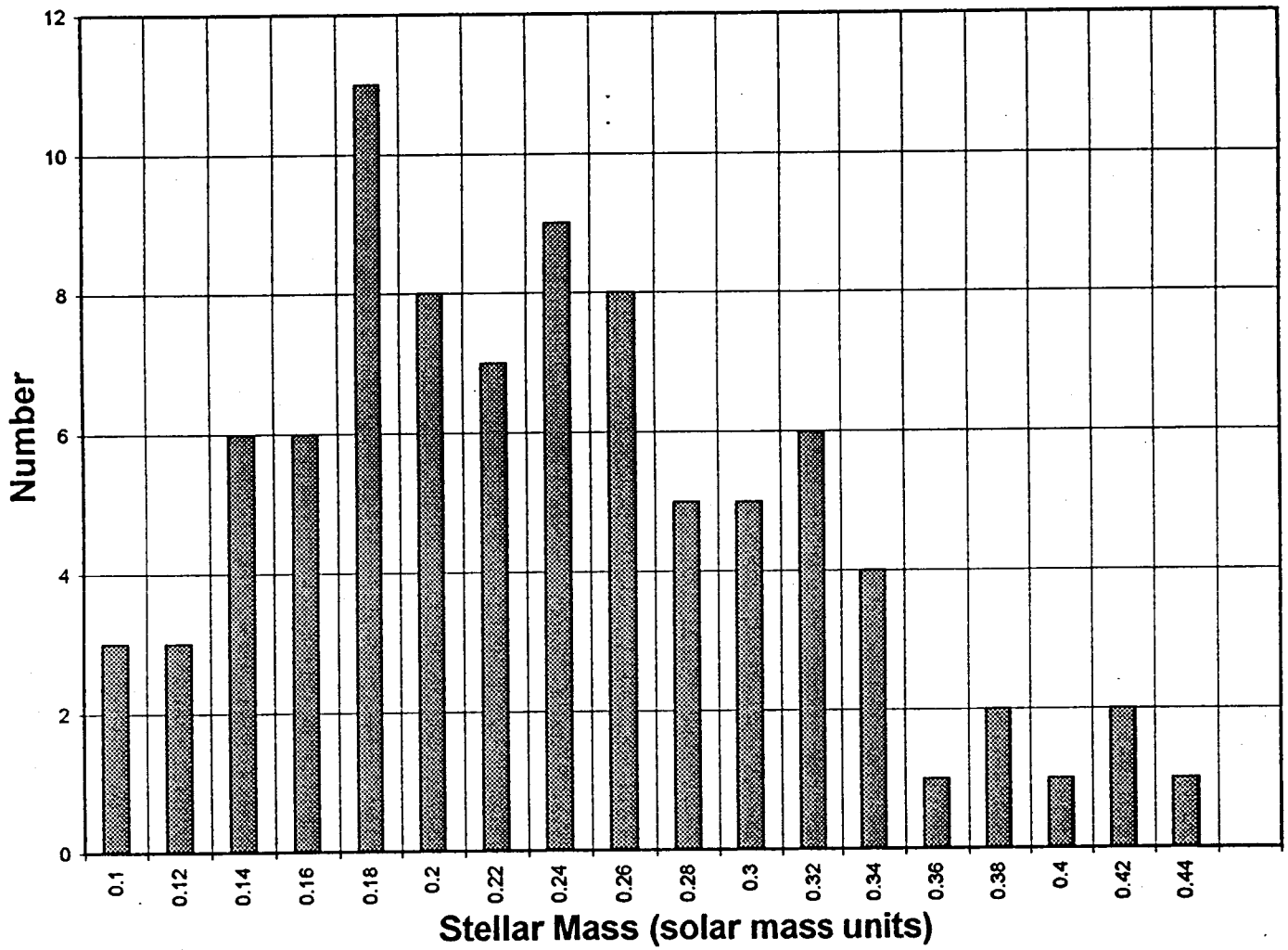

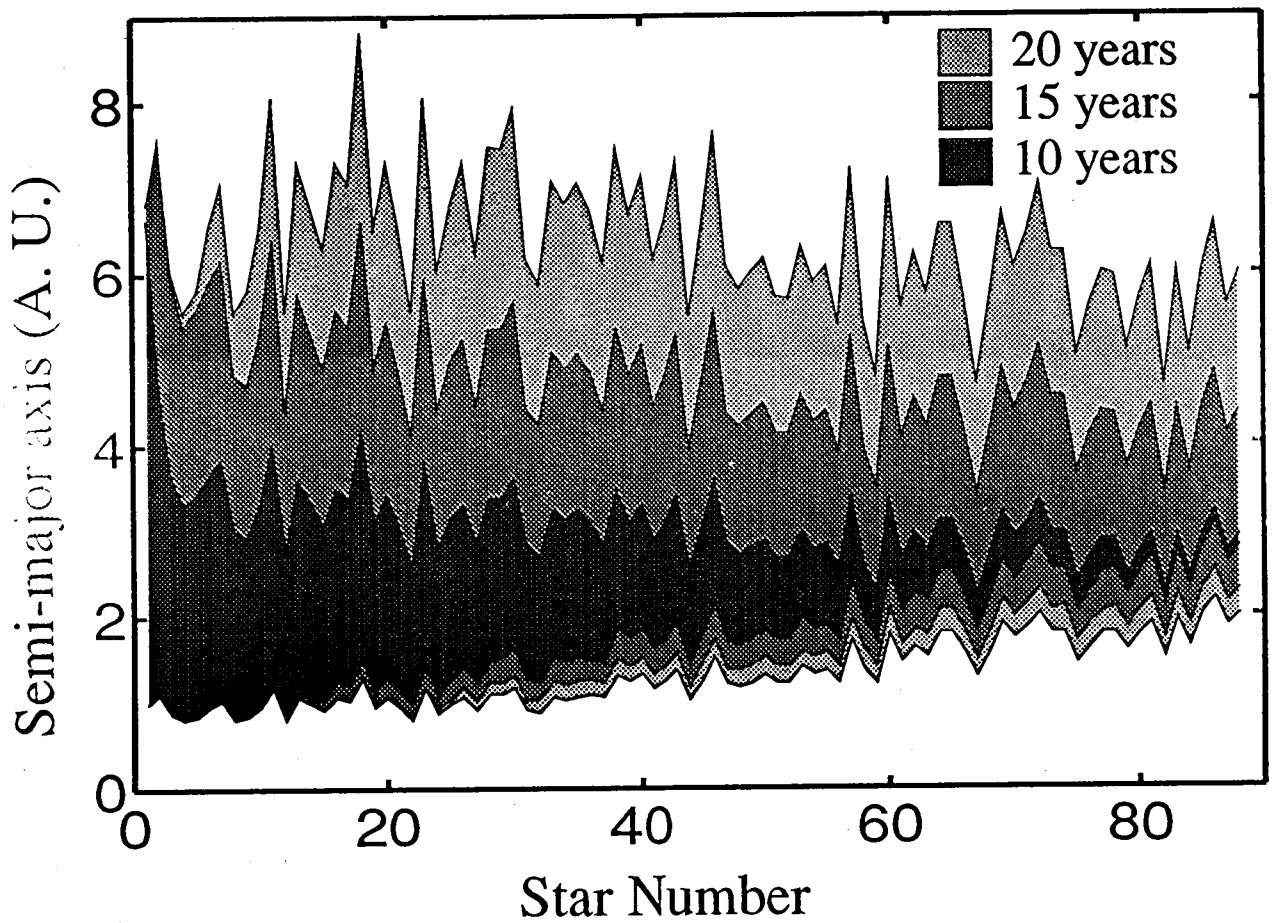
20 years
15 years
10 years
Semi-major axis (A. U.)
0
2
4
6
8
0
20
40
60
80
Star Number

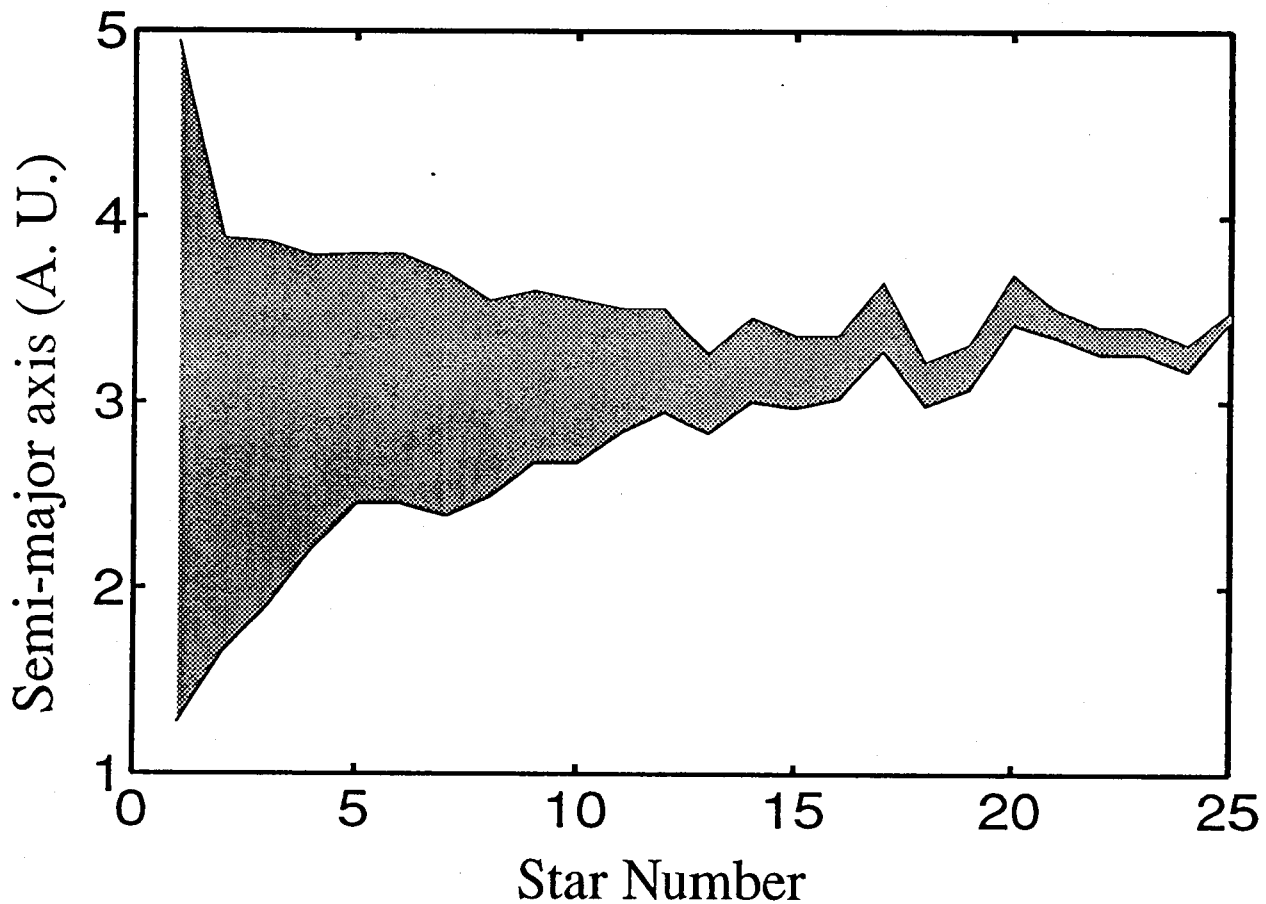
Semi-major axis (A. U.)
5
4
3
2
1
0
5
10
15
20
25
Star Number

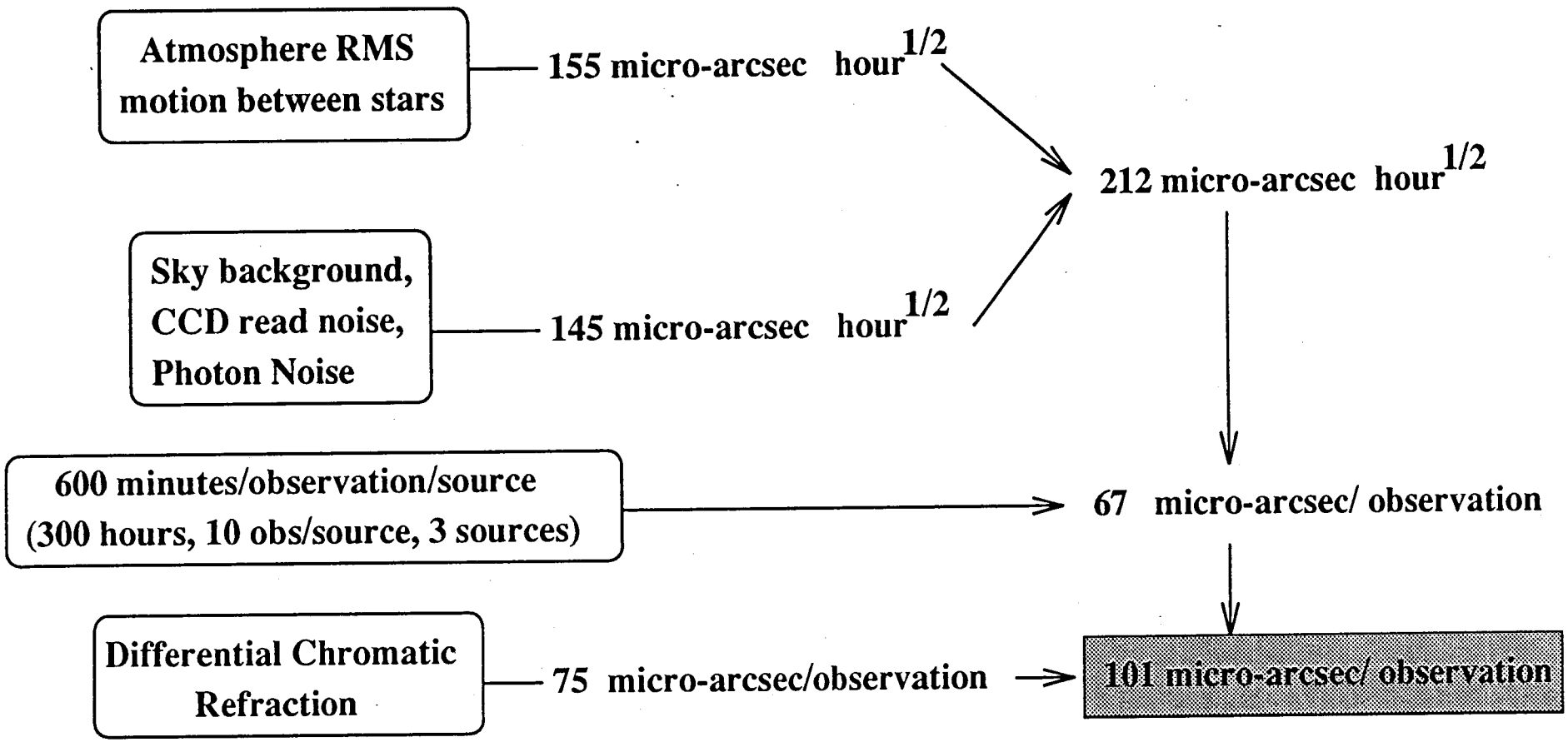
Atmosphere RMS motion between stars
155 micro-arcsec hour^1/2
Sky background, CCD read noise, Photon Noise
145 micro-arcsec hour^1/2
212 micro-arcsec hour^1/2
600 minutes/observation/source (300 hours, 10 obs/source, 3 sources)
67 micro-arcsec/ observation
Differential Chromatic Refraction
75 micro-arcsec/observation
101 micro-arcsec/ observation